Enhanced Organic Pollutant Adsorption Using Zeolite-Carbon Dots Composites Synthesized by the Impregnation Method

Ho Tan Thanh[1,2,3], Nguyen Thien Phuc[4], Dang Dinh Khoi[4], and Nguyen Quang Long[1,2*]

[1]*Faculty of Chemical Engineering, Ho Chi Minh City University of Technology (HCMUT), 268 Ly Thuong Kiet Street, Ho Chi Minh City 700000, Viet Nam*

[2]*Vietnam National University Ho Chi Minh City, Linh Trung Ward, Ho Chi Minh City 700000, Viet Nam*

[3]*Ho Chi Minh City University of Industry and Trade, 140 Le Trong Tan Street, Tay Thanh Ward, Ho Chi Minh City 700000, Viet Nam*

[4]*Ho Chi Minh City University of Technology and Education, 01 Vo Van Ngan Street, Ho Chi Minh City 700000, Viet Nam*

**** Corresponding author:***

tel: +84-9665417
email: nqlong@hcmut.edu.vn

Received: August 17, 2025
Accepted: November 27, 2025

DOI: 10.22146/ijc.110466

Abstract: *In this study, a novel zeolite–carbon dots (ZCD) composite was synthesized via impregnation to enhance the adsorption performance of zeolite. The attachment of carbon dots (CDs) onto the zeolite surface was confirmed by SEM/EDS, TEM, BET, and FT-IR analyses. These results showed that CDs were uniformly dispersed on the FAU-type zeolite, introduced additional –OH, $–CH_x$, and $–NH_2$ groups, and increased the BET surface area from 444.5 to 491.5 $m^2\ g^{-1}$. The presence of functional groups on the surface of CDs enhanced the adsorption capacity of zeolite. Notably, ZCD exhibited a 45% higher adsorption capacity for methylene blue (MB) than pristine zeolite, with a maximum experimental uptake of 32.53 mg g^{-1}. Adsorption isotherm and kinetic studies, best described by the Langmuir model (q_m = 29.22 mg g^{-1}, R^2 = 0.9815) and the pseudo-second-order kinetic model (R^2 = 0.9991), indicated that MB uptake on ZCD occurred through both physical and chemical interactions. These results suggest that the ZCD composite is a promising adsorbent for the removal of organic dyes in water treatment applications.*

Keywords: *zeolite composite; carbon dots; methylene blue; wastewater treatment; impregnation method*

■ INTRODUCTION

Water pollution from industrial activities, especially in the textile dyeing sector, is becoming increasingly severe, primarily due to the discharge of organic dyes into the environment. These dyes possess complex molecular structures, are highly stable under natural conditions, and exert harmful effects on both the environment and human health. Among them, methylene blue (MB) is a commonly used dye characterized by its distinctive blue color. MB at high concentrations in water can inhibit oxygen uptake, adversely affect the reproduction of aquatic organisms, and disrupt microbial activity, thereby interfering with natural purification processes and reducing water quality [1-2]. Ecotoxicity data suggest that MB poses environmental risks even at very low concentrations. For example, in *Daphnia magna*, the reported EC_{50} (48 h) is 61.5 ± 2.3 μg L^{-1} and LC_{50} (24 h) is 149.0 ± 2.2 μg L^{-1}, with a chronic NOEC of approximately 4.7 μg L^{-1}, indicating potential toxicity in sensitive aquatic organisms [3]. In aquaculture, although MB is commonly used for bath treatments at concentrations of 2–3 mg L^{-1}, toxic effects have been observed at comparable levels, such as 2 mg L^{-1} for 21 days in goldfish and 5 mg L^{-1} in angelfish larvae [4-5]. Consequently, regulatory frameworks such as the EU's RPA for unauthorized dyes and the U.S. FDA's HACCP guidelines for aquaculture recognize MB as a chemical hazard requiring stringent control throughout the supply chain [6-7]. In humans, MB exposure at high doses may cause adverse effects, including hemolysis

(especially in individuals with G6PD deficiency), methemoglobinemia, and drug interactions via reversible MAO-A inhibition. These potential risks underscore the importance of minimizing residual MB in treated water to prevent accumulation in edible aquatic organisms [8]. Among current wastewater treatment technologies, such as adsorption, chemical treatment, and ion exchange, adsorption is considered an efficient, effective, and cost-saving method [9].

Zeolite is a widely used adsorbent material characterized by its porous structure and uniform microporous channel system, which provides a high surface area and good adsorption performance at a low cost [10-11]. However, due to their small pore sizes (in the Angstrom range), conventional zeolites often struggle to adsorb large organic molecules such as MB [12]. Several studies have applied zeolite modification techniques to improve their adsorption capacity. For instance, zeolite has been modified with ethanolamine [13] or functionalized with organic acids to generate mesoporous systems [14]. Ramutshatsha-Makhwedzha et al. [15] successfully synthesized a Fe_3O_4@TiO_2@zeolite nanocomposite to enhance the adsorption performance of zeolite, while the group of Tubon-Usca et al. [16] incorporated graphene oxide into zeolite to improve its efficiency in removing MB from wastewater.

Moreover, carbon nanomaterials, especially carbon dots (CDs), are gaining attention in water treatment due to their ultra-small size (< 10 nm), large surface area, and numerous functional groups, such as –OH, –COOH, and $–NH_2$ [17]. CDs exhibit high efficiency in treating organic pollutants, including MB [18]. However, due to their small size and low content, it is challenging to apply CDs in practice without combining them with carrier materials. Many studies have successfully synthesized composite materials [19], CDs on polymer composite materials [20], with enhanced adsorption performance through multivalent surface interactions [1,21]. However, these composite synthesis methods primarily employ thermal, sol-gel, or microwave-assisted techniques, which typically require stringent conditions and high costs [22]. The impregnation method stands out as a simple, scalable, and environmentally friendly solution, making it especially suitable for immobilizing CDs onto inorganic materials, such as zeolite. Nevertheless, the number of studies on zeolite-CD (ZCD) composites prepared by impregnation remains limited, and in-depth research on the relationships among material characteristics, adsorption capacity, kinetics, and adsorption thermodynamics in this system is still lacking. In this study, a composite was synthesized by impregnating zeolite with CDs, with different mixing ratios investigated to determine the optimal conditions for ZCD adsorption of MB in aqueous solution. The results showed that the ZCD material exhibited superior adsorption performance compared to pure zeolite. The synthesized material was then subjected to kinetic and isotherm adsorption modeling to further analyze the interaction mechanism between ZCD and MB, contributing to a deeper understanding of the relationship between the zeolite pore structure and the rich functional groups of CDs in removing organic pollutants.

■ EXPERIMENTAL SECTION

Materials

In this study, *m*-phenylenediamine (99%, Aladdin Co.), sulfamic acid (99%, Damas-Beta Co.), and ethylene glycol (99%, Sinopharm Co.) were used to synthesize CDs. At the same time, zeolite (Z) was obtained using the procedure described in our previously reported publication [14].

Instrumentation

The morphology and pore structure of the material were examined using a scanning electron microscope (SEM, JSM IT-200, JEOL, Japan) and a transmission electron microscope (TEM, JEM-1010, JEOL, Japan), respectively. The crystalline structure was analyzed by X-ray diffraction (XRD; Bruker D2 Phaser, Germany; CuKα), and the specific surface area was determined by the nitrogen adsorption–desorption method (Brunauer-Emmett-Teller (BET); Nova Station C, Quantachrome Instruments, USA). The elemental composition and chemical functional groups were characterized by energy-dispersive X-ray spectroscopy (EDS) and Fourier-transform infrared spectroscopy (FTIR, Jasco

FT/IR-4700, Japan). Thermal stability was evaluated by thermogravimetric analysis (TGA) and differential scanning calorimetry (DSC) using a Q500 and a Q20 instrument (TA Instruments, USA). In addition, the photoluminescence spectrum of CDs was measured using a Horiba Fluoromax Plus spectrometer (Horiba, Japan).

Procedure

Zeolite-carbon dots synthesis

The process for fabricating the adsorbent involves synthesizing CDs and the zeolite-CD composite. Firstly, CDs were synthesized by solvent thermal reflux using *m*-phenylenediamine and sulfamic acid as precursors in ethylene glycol. The reaction temperature for the fabrication of CDs was maintained at 160 °C for 2 h to obtain a CD solution. The adsorbent was synthesized by wet impregnation using a CD solution and zeolite. In a typical process, 2 g of Z was added to 100 mL of distilled water in a 250 mL Erlenmeyer flask, and the mixture was stirred. Then, the as-prepared CDs were added with different weight ratios surveyed (1, 3, 7, and 10%). After that, the mixture was continuously stirred at room temperature for 4 h using a magnetic stirrer at 400 rpm. Next, the mixture was thoroughly washed several times with distilled water by centrifugation to remove excess CDs. The resulting solid samples, after drying at 80 °C for 24 h, were labeled as ZxCD, with x = 1, 3, 7, and 10 corresponding to the percentage of CDs in the surveyed ratios.

Evaluation of adsorption performance

The experiment evaluating the adsorption efficiency of composite samples synthesized at different Z/CD ratios and the control sample (Z0CD) was conducted in 250 mL Erlenmeyer flasks containing 150 mL of a 50 ppm MB solution, with an adsorbent dosage of 1 g/L in each experiment. The mixture was stirred at 200 rpm and room temperature (30 ± 2 °C) for 4 h. The samples were centrifuged before measuring the MB concentration to minimize interference from the composite. Each experiment was repeated three times under the same conditions, and the results were reported as mean values with standard deviation (error bars). The MB concentration was determined by UV-vis spectrophotometry (V-730, JASCO, Japan) at 663 nm. The adsorption efficiency H% was calculated according to Eq. (1);

$$H\% = \frac{C_0 - C_t}{C_0} \times 100\% \quad (1)$$

where C_0 is the initial concentration of MB (ppm), and C_t is the MB concentration at time t (ppm).

Adsorption isotherm studies

To determine the adsorption isotherm equations, experiments were conducted with different initial concentrations (30, 50, 80, and 100 ppm). The equilibrium adsorption capacity (q_e) was calculated using Eq. (2);

$$q_e = \frac{(C_0 - C_e)V}{m} \quad (2)$$

where V is the volume of MB solution (L), m is the adsorbent mass (g), C_0 and C_e are the initial and equilibrium concentrations of MB (ppm), respectively. The Langmuir and Freundlich models were used to investigate adsorption, as shown in Table 1.

Adsorption kinetics studies

The adsorption kinetics of MB onto the composite were investigated by monitoring the variation in the amount of adsorbed MB (q_t, mg/g) over time t, calculated according to Eq. (3).

$$q_t = \frac{(C_0 - C_t)V}{m} \quad (3)$$

Two kinetic models were applied in this study: the pseudo-first-order and pseudo-second-order models, as presented in Table 2.

Table 1. Two isotherm models for the adsorption process of MB

Models	Nonlinear expression	Linear form
Langmuir	$q_e = \frac{q_m.K_L.C_e}{1+K_L.C_e}$	$\frac{C_e}{q_e} = \frac{1}{q_m.K_L} + \frac{C_e}{q_m}$
Freundlich	$q_e = K_F.C_e^{\frac{1}{n}}$	$\log q_e = \log K_F + \frac{1}{n}\log C_e$

Table 2. Mathematical expressions and units of kinetic models used for MB adsorption

Models	Nonlinear expression	Linear form
Pseudo-first-order	$q_t=q_e(1-e^{-k_1.t})$	$\ln(q_e-q_t)=\ln q_e-k_1.t$
Pseudo-second-order	$q_e=\frac{q_e^2.k_2.t}{1+k_2.q_e.t}$	$\frac{1}{q_t}=\frac{1}{k_2.q_e}+\frac{t}{q_e}$

■ RESULTS AND DISCUSSION

Adsorption Experiments

Effect of Z/CDs ratio on adsorption performance

The adsorption experiments investigating the MB adsorption capacity of the composite materials were conducted over a period of 4 h under the following conditions: solid-to-liquid ratio of 1 g/L and initial MB concentration of 50 ppm (Fig. 1), presenting the MB removal efficiency of zeolite/CDs composite samples at different ratios compared to the control sample (original sample) without CDs (Z0CD). The results indicated that the combination of CDs and zeolite significantly improved the adsorption efficiency.

Specifically, the Z7CD sample exhibited the highest adsorption efficiency (62.6%) among all samples, consistent with an optimal CD loading. When the CD content was increased to 10% (Z10CD), the efficiency decreased to 47.2% (Fig. 1). We attribute this decline to a surface-coverage (pore-blocking) effect that limits dye diffusion into the composite's pore network [13,16], in line with reports that dye uptake on zeolitic adsorbents depends on accessible porosity [12]. In general, these results show that the presence of CDs significantly enhances the adsorption capacity of zeolite for MB, which can be attributed to the functional groups on the CD surface that provide favorable sites for interaction with MB molecules. Due to its superior adsorption capacity, Z7CD was selected for comprehensive characterization to establish correlations among its structure, properties, and adsorption performance. Supporting this, adsorption isotherm models and kinetic studies were conducted with this sample to clarify the interaction mechanism between ZCD and MB, providing in-depth insights into the synergistic role between the zeolite pore structure and the CD surface functional groups.

Effect of solid/liquid ratio on adsorption efficiency

A total of five samples, each containing 150 mL of MB solution at an initial concentration of 50 ppm, were prepared with different ZCD/MB solid-to-liquid ratios of 0.5, 0.7, 1.0, 1.3, and 1.5 g/L. These samples were continuously stirred at 200 rpm under ambient temperature, and the equilibrium concentration was measured after 210 min. The MB concentration at equilibrium are presented in Table 3. Fig. 2 shows the effect of the solid/liquid (S/L) ratio on MB adsorption efficiency. When the S/L ratio increased from 0.5 to 1.0, the removal efficiency (H%) increased significantly

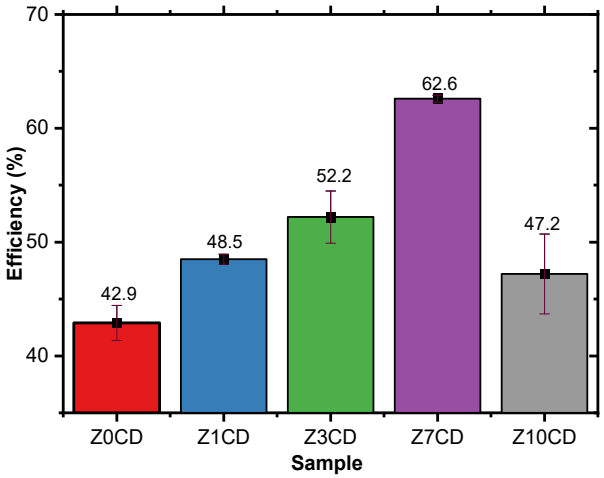

Fig 1. MB adsorption efficiency of the composite samples

Table 3. Effect of solid/liquid ratio on MB adsorption efficiency

S/L Ratio	C_{MB} (ppm)	H%
0.5	31.2	37.6
0.7	21.8	56.4
1.0	18.7	62.5
1.3	18.7	62.7
1.5	18.5	63.0

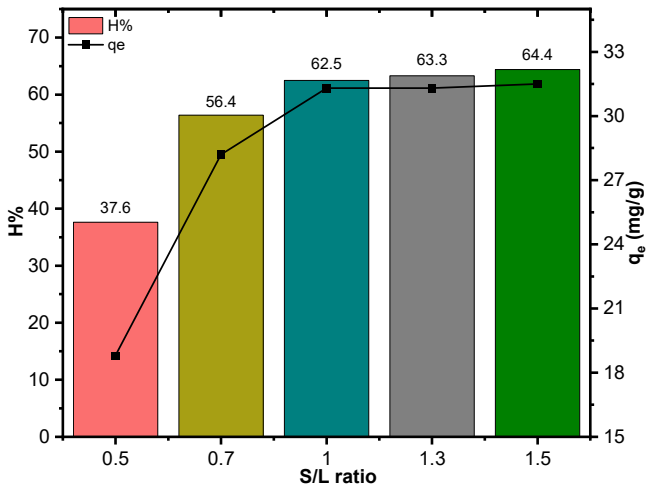

Fig 2. Effect of solid/liquid ratio on MB removal and q_e

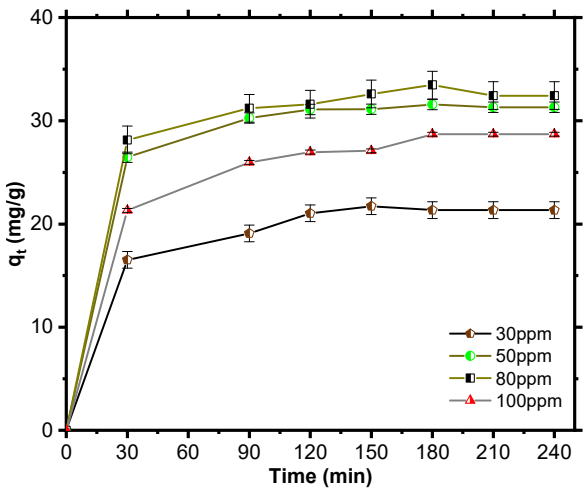

Fig 3. q_t vs. time for MB adsorption on Z7CD

from 37.6 to 62.5%, and the adsorption capacity at equilibrium (q_e) also increased sharply from about 18.0 to 31.3 mg/g. This was due to the increased amount of adsorbent, resulting in a better adsorption capacity. However, when the S/L was further increased to 1.5, the H% only increased slightly to 64.4%, and q_e remained almost unchanged. This was due to the excessive amount of adsorbent, which reduced the amount of MB adsorbed per unit mass, resulting in no noticeable effect. Therefore, the S/L ratio of 1.0 is considered optimal, ensuring both high adsorption efficiency and effective use of materials without waste.

Adsorption isotherm and kinetics

The adsorption isotherm experiments of Z7CD with MB were conducted over 4 h under the following conditions: a solid-to-liquid ratio of 1 g/L and initial MB concentrations of 30, 50, 80, and 100 ppm. The results (Fig. 3) showed that adsorption of methylene blue (MB) onto the composite material occurred rapidly over the first 30 min and reached equilibrium after approximately 150 min. The equilibrium adsorption capacities at initial MB concentrations of 30, 50, 80, and 100 ppm were 21.37, 31.28, 32.53, and 27.87 mg/g, respectively. The increasing q_t values with higher initial MB concentrations indicated that more MB molecules could access and interact with the adsorbent's active sites, and that the diffusion driving force into the more porous structure was enhanced. However, when the concentration exceeded a certain threshold (at 100 ppm), the adsorption capacity tended to decrease. This may be attributed to rapid saturation of the adsorbent surface's active sites, reducing the number of vacant sites, along with the aggregation of MB molecules at high concentrations [23], which potentially hinders diffusion into smaller micropores and results in non-continuous improvement in adsorption performance.

The parameters of the Langmuir and Freundlich models for the adsorption of MB onto Z7CD at 30 ± 2 °C are presented in Table 4, derived from the regression curves in Fig. 4. The Langmuir adsorption isotherm model has a linear correlation coefficient R^2 of 0.9815, which is higher than that of the Freundlich model (0.4135), indicating that the Langmuir model is more suitable for describing the MB adsorption process onto Z7CD. The results also suggest that the MB adsorption

Table 4. Summary of adsorption isotherm parameters

Isotherm models	Parameter value	
Langmuir	Slope	0.03423 ± 0.00033
	Intercept	0.00279 ± 0.00017
	q_m (mg g^{-1})	29.22
	K_L (L mg^{-1})	12.27
	R^2	0.9815
Freundlich	Slope	1.26176 ± 0.15
	Intercept	0.12803 ± 0.10
	K_F [(mg g^{-1}) (L $mg^{-1})^{1/n}$]	
	n	7.81
	R^2	0.4135
q_e (mg g^{-1})		32.53

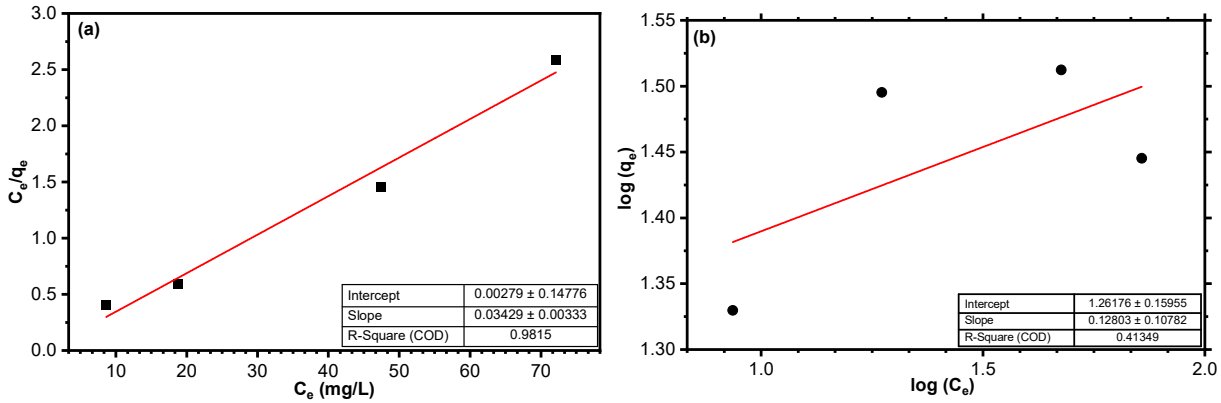

Fig 4. (a) Langmuir and (b) Freundlich isotherm plots

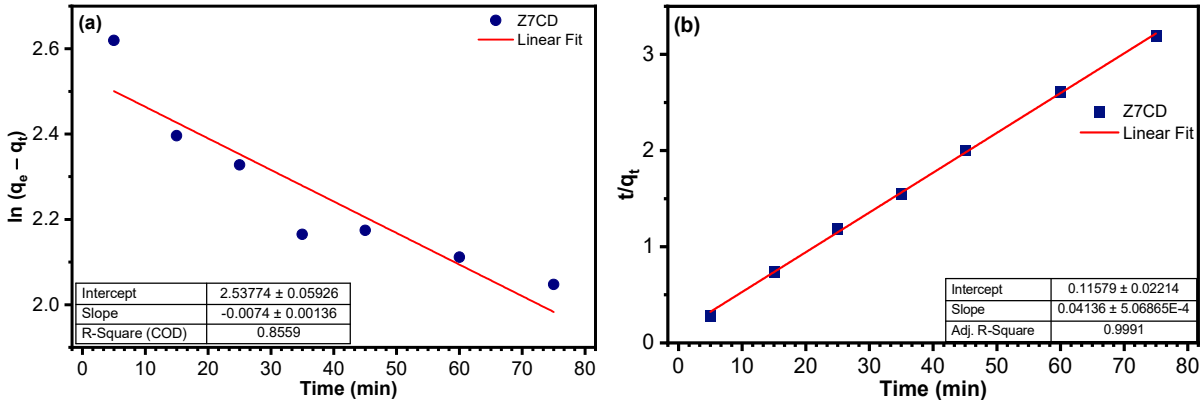

Fig 5. (a) Pseudo-first-order kinetics and (b) pseudo-second-order kinetics for MB adsorption by Z7CD

Table 5. Summary of kinetic parameters

Models	Parameter value	
Pseudo-first-order	Slope	−0.0074 ± 0.00136
	Intercept	2.53774 ± 0.05926
	k_1 (min^{-1})	0.0074
	q_e (mg g^{-1})	12.64
	R^2	0.8559
Pseudo-second-order	Slope	0.04136 ± 0.00057
	Intercept	0.11579 ± 0.02214
	k_2 (g mg^{-1} min^{-1})	0.01483
	q_e (mg g^{-1})	24.17
	R^2	0.9991
q_{exp} (mg g^{-1})		32.53

process may be chemisorption, which is related to surface functional groups and binding energy [24].

Adsorption kinetic experiments of Z7CD with MB were conducted over the first 75 min. The experimental data were processed and fitted using the pseudo-first-order and pseudo-second-order kinetic models, as illustrated in Fig. 5. The values of q_e and k_1 in the first-order model, as well as k_2 in the second-order model, were determined from the slope and intercept of the linear plots. The results are presented in Table 5.

Table 5 shows that the pseudo-second-order kinetic model (R^2 = 0.9991) provides a better description of the adsorption process than the first-order model (R^2 = 0.8559). Moreover, the adsorption process fits the Langmuir adsorption model (monolayer adsorption), indicating that the mechanism is predominantly chemisorption between the composite and MB.

Material Characterization

Optical properties of carbon dots

The as-prepared CDs were characterized for their optical properties using UV-vis and photoluminescence (PL) spectroscopy. The UV-vis spectrum of the synthesized CDs (red curve) exhibited a strong absorption peak at approximately 280 nm, indicating the π→π* transition of C=C bonds in the aromatic ring. In addition, the shoulder around 450 nm suggests the

n→π* transition of C=O or N–C=O. The PL spectrum of CDs exhibited a sharp emission peak at approximately 510 nm upon excitation at 495 nm, indicating that the CDs are green-emitting, as shown in the digital image in Fig. 6.

Characteristics of composite materials

The FTIR spectra of Z0CD and Z7CD are presented in Fig. 7. It is observed that both samples exhibit characteristic absorption bands at 3360, 2360, 1646, 969, 560, and 450 cm^{-1}, which are typical for FAU-type zeolite. Among them, the broad absorption band at 3360 cm^{-1} is assigned to the stretching vibration of –OH groups, indicating the presence of adsorbed water molecules or surface hydroxyl groups (Si–OH, Al–OH) in the zeolite framework. The band at 2360 cm^{-1} is assigned to the stretching vibration of CO_2 molecules physically adsorbed within the material's porous structure [25]. The band at 1646 cm^{-1} is attributed to the bending vibration of H_2O molecules adsorbed inside the zeolite structure [26]. Likewise, the stretching vibration of the Si–O–Al bond produces a band around 969 cm^{-1}, and the band at 560 cm^{-1} corresponds to the bending vibration of Al–O–Si linkages, confirming the presence of aluminosilicate bonds, which are the principal component of FAU-type zeolite [27]. The absorption band at 540 cm^{-1} is a characteristic signal of the external linkage vibration of TO_4 tetrahedra (where T is Al or Si) at the edge sites of FAU-type zeolite with strong intensity, contributing to the identification of highly crystalline zeolite phases in the composite. The band at 674 cm^{-1} is related to out-of-plane vibrations of Si–O or Al–O groups in the zeolite framework. Thus, the characteristic absorption bands in the FTIR spectra confirm the presence of functional groups and typical framework structures of FAU-type zeolite in both composite samples.

In addition, the FTIR spectrum of the Z7CD composite sample shows several distinct absorption bands, clearly reflecting the presence of surface functional groups originating from CDs. Two bands at 2983 and 2900 cm^{-1} correspond to the stretching vibrations of C–H bonds in methyl or methylene groups, characteristic of hydrocarbon chains in the CD structure. Furthermore, the band at 1646 cm^{-1}, in addition to being assigned to the

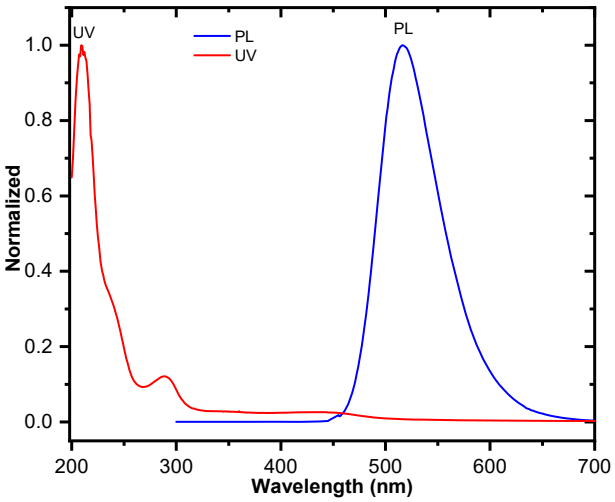

Fig 6. Photoluminescence (PL) and UV–vis absorption spectra of CDs

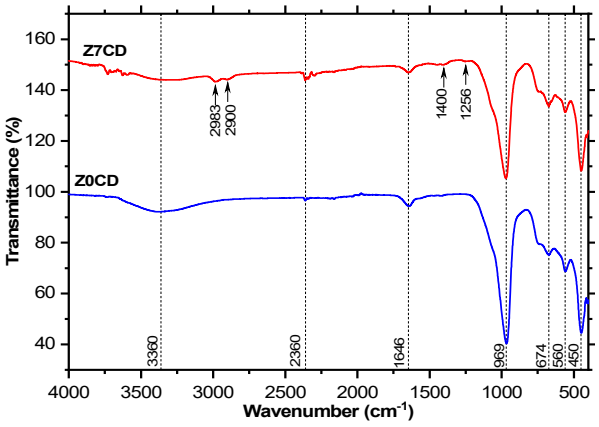

Fig 7. FTIR spectra of Z0CD and Z7CD

bending vibration of adsorbed H_2O molecules, may also correspond to the N–H bending vibration of amine groups, as indicated by the simultaneous appearance of bands at 1400 and 1256 cm^{-1}, which match the bending and stretching vibrations of C–N bonds [28], clearly confirming the presence of $–NH_2$ groups on the Z7CD material. This finding is entirely consistent with the precursors used in the synthesis of CDs (*m*-phenylenediamine and sulfamic acid), both of which are rich in primary amine groups ($–NH_2$). In general, the appearance of characteristic bands such as free –OH groups, hydrocarbon groups ($–CH_3$, $–CH_2–$), and nitrogen-containing functional groups ($–NH_2$) in the FTIR spectrum of Z7CD partially confirms the bonding of CDs to the zeolite framework. These functional groups

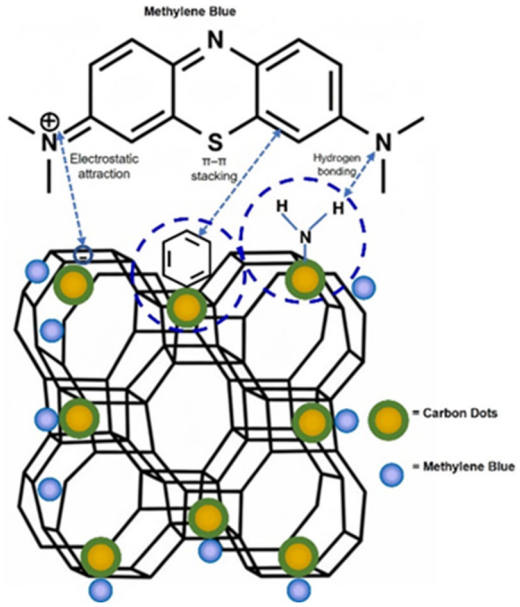

Fig 8. MB chemisorption on the composite

play a crucial role in chemisorption by forming electrostatic attractions, hydrogen bonds, and π–π interactions between the composite surface and MB molecules (Fig. 8).

SEM images (Fig. 9) show that both Z0CD and Z7CD exhibit a block-like morphology with well-defined edges and tight aggregation. The Z7CD sample appears rougher, with more areas exhibiting surface fragmentation. The composite surface exhibits finer features with particle sizes of approximately 50 nm, indicating that the CDs are successfully bonded to the zeolite surface. In addition, EDS analysis (Fig. 10) provides elemental information indicating the presence of carbon, nitrogen, and sulfur (C, N, and S), confirming the presence of CDs on the composite material's surface.

Furthermore, the TEM image (Fig. 11) of the Z7CD composite sample reveals a crystalline network structure and a clearly visible system of mesoporous channels, both of which are typical characteristics of zeolites. This confirms that the hydrothermal synthesis of zeolite was effective and well-maintained throughout

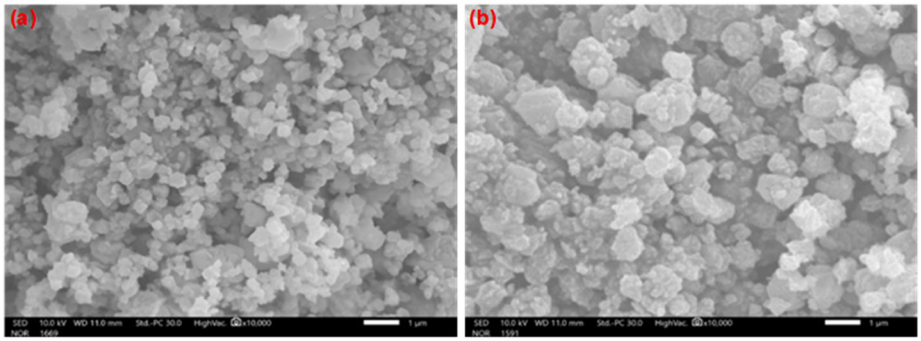

Fig 9. SEM image of (a) Z0CD and (b) Z7CD sample

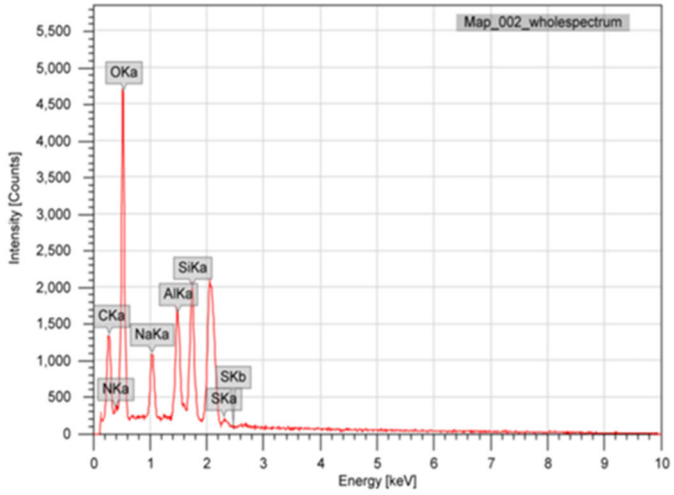

Element	Mass% (±)	Atom% (±)
C	24.91 ± 0.15	35.15 ± 0.22
N	1.56 ± 0.08	1.88 ± 0.09
O	38.78 ± 0.23	41.08 ± 0.24
Na	6.11 ± 0.11	4.50 ± 0.08
Al	10.33 ± 0.15	6.49 ± 0.09
Si	16.27 ± 0.20	9.82 ± 0.12
S	2.06 ± 0.09	1.09 ± 0.05
Total	100.00	100.00

Fig 10. EDS analysis of Z7CD

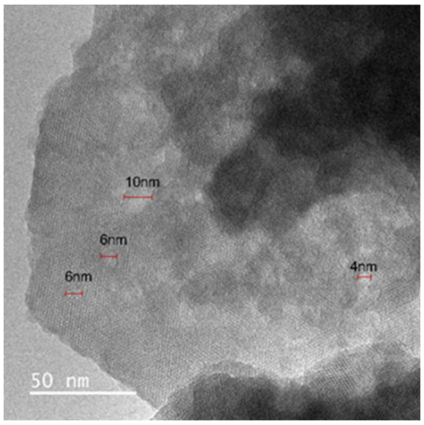

Fig 11. TEM image of the Z7CD composite sample

the composite formation process. Small, dark dots with high contrast, approximately 4–10 nm in size, are dispersed across the zeolite surface, further indicating the presence of CDs. The morphological and elemental composition analysis by SEM/EDS, combined with TEM imaging and FTIR spectra, clearly demonstrates that CDs were successfully attached to the zeolite surface without destroying its characteristic mesoporous structure. This confirms the effectiveness of the composite synthesis process between zeolite and CDs.

The XRD patterns shown in Fig. 12 reveal characteristic diffraction peaks of FAU-type zeolite at 2θ = 9.96°, 11.68°, 15.38°, 23.22°, and 33.46°, observed in all synthesized samples, including both the parent zeolite (Z0CD) and the composite sample (Z7CD). This indicates that the zeolite synthesis process and subsequent composite formation retained the zeolite framework's crystalline structure. Furthermore, no additional impurity peaks were observed, indicating that the synthesis process was effective and did not generate any undesired secondary phases. Overall, the XRD patterns suggest that the obtained composite exhibits the typical FAU-type zeolite structure, and the incorporation of CDs does not disrupt the crystalline framework.

The nitrogen adsorption–desorption isotherms of the two samples Z0CD and Z7CD (Fig. 13) both exhibit the characteristic features of mesoporous materials, with a hysteresis loop beginning to appear at around P/P_0 = 0.45 and becoming more evident in the range of 0.8–1.0, consistent with type IV according to the IUPAC classification. The Z7CD sample exhibits higher nitrogen adsorption across the entire pressure range, indicating a larger specific surface area. The results from Table 6 show that the BET surface area of Z7CD is 491.5 m^2/g, higher than that of Z0CD (444.5 m^2/g). This indicates the successful incorporation of CDs into the zeolite, increasing the number of potential adsorption sites and the specific surface area, thereby improving the adsorption efficiency for organic pollutants such as MB.

TGA/DSC analysis is presented in Fig. 14. For the Z0CD sample, the TGA curve shows a major weight loss of approximately 23.8%, primarily due to the evaporation of physically adsorbed water and water confined in the mesopores of the zeolite framework. These data are supported by a thermal endothermic peak on the DSC curve at 170.3 °C with an associated enthalpy

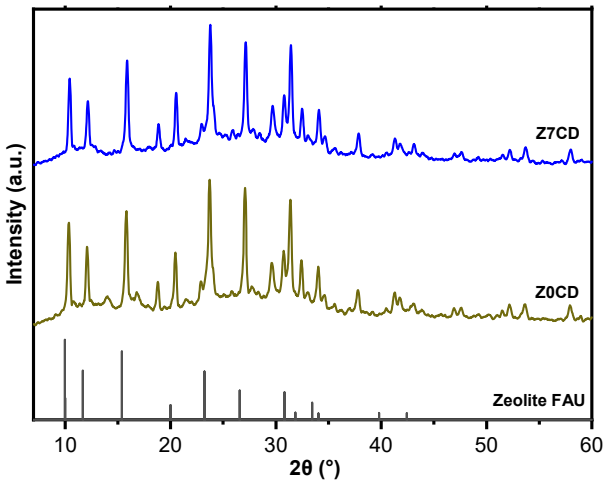

Fig 12. XRD patterns of zeolite and composite

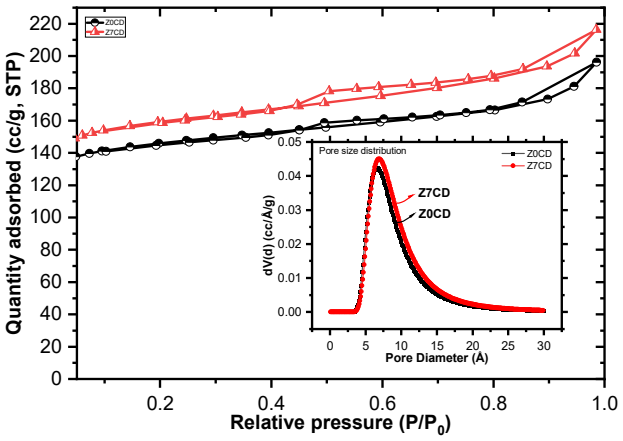

Fig 13. Nitrogen adsorption–desorption isotherms of Z0CD and Z7CD

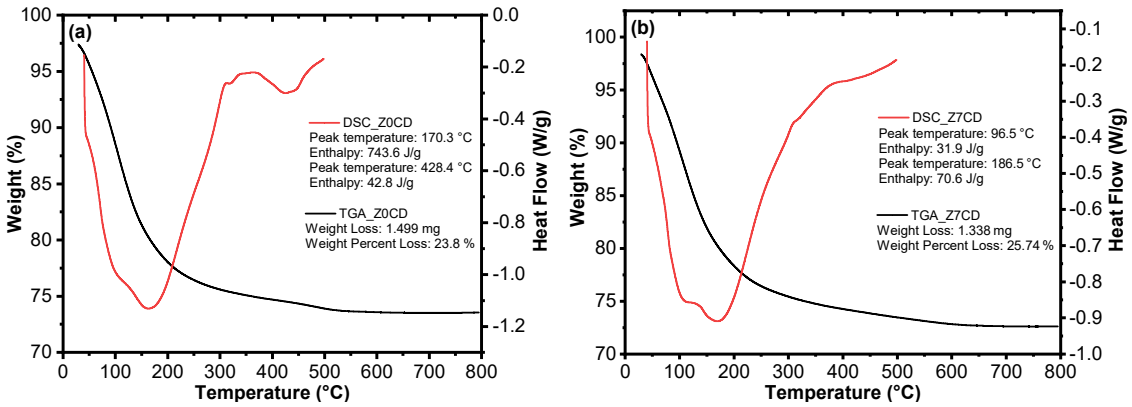

Fig 14. TGA/DSC curves of (a) Z0CD and (b) Z7CD samples

Table 6. Summary of the physical properties of zeolite Z0CD and composite Z7CD

Sample	S_{BET} (m^2/g)	S_{micro} (m^2/g)	$S_{external}$ (m^2/g)	V_{total} (cm^3/g)	V_{micro} (cm^3/g)
Z0CD	444.5	373.8	70.7	0.30	0.19
Z7CD	491.5	406.4	85.1	0.33	0.20

of 743.6 J/g. Additionally, a second endothermic peak appears at 428.4 °C with an enthalpy of 42.8 J/g, likely due to a slight structural rearrangement or the minor decomposition of residual impurities. Overall, Z0CD demonstrates high thermal stability and contains virtually no organic components, which is characteristic of conventional FAU-type zeolite. In contrast, the Z7CD sample exhibits a higher total weight loss of 25.74% compared to the Z0CD sample. This increase is attributed to a CD layer coating the surface, which contains volatile components and hydrophilic functional groups (e.g., –OH, C=O, N–H) that tend to decompose at moderate temperatures. The DSC curve displays two distinct endothermic peaks. The first peak at 96.5 °C (ΔH = 31.9 J/g) corresponds to the evaporation of physically adsorbed water and labile surface groups. The second peak at 186.5 °C (ΔH = 70.6 J/g) corresponds to the decomposition of surface functional groups on CDs, confirming the successful attachment of CDs to the zeolite. Nevertheless, no strong exothermic signals or drastic weight loss are observed up to 500 °C in either sample, indicating that both the parent zeolite and the Z7CD composite exhibit good thermal stability, making them suitable for practical applications. Based on the weight-loss results for Z7CD and Z0CD, the amount of CDs grafted onto the zeolite was estimated to be approximately 1.94% by weight. With a mixing ratio of 7% used during the synthesis of Z7CD, this indicates that the CD grafting efficiency onto zeolite reached approximately 28.6%. This level of retention agrees with prior CD/composite reports, where weakly bound species are removed during purification and pore size/site-saturation effects limit attainable loading, so the actual retained amount seldom matches the nominal feed [19-20,22].

■ CONCLUSION

In this study, a novel composite material was successfully synthesized by incorporating CDs onto Z via a wet impregnation method, as revealed by the analytical techniques. The presence of characteristic functional groups from CDs on the material surface was confirmed, which significantly enhanced the adsorption efficiency of MB (an increase of 45.9%) compared to the parent zeolite, with a maximum experimental adsorption capacity of 32.53 mg g^{-1}. The adsorption process was well described by the Langmuir isotherm and pseudo-second-order kinetics models. Therefore, the composite exhibits great potential for removing MB, providing a promising and practically applicable approach to treat wastewater containing persistent organic pollutants.

■ ACKNOWLEDGMENTS

We acknowledge Ho Chi Minh City University of Technology (HCMUT), VNU-HCM, and Ho Chi Minh

City University of Industry and Trade for supporting this study.

■ CONFLICT OF INTEREST

The authors declare that they have no conflict of interest.

■ AUTHOR CONTRIBUTIONS

Conceptualization: Ho Tan Thanh, Dang Dinh Khoi, Nguyen Quang Long; Methodology: Ho Tan Thanh, Dang Dinh Khoi; Formal analysis and investigation: Nguyen Thien Phuc, Dang Dinh Khoi; Writing – original draft preparation: Ho Tan Thanh, Dang Dinh Khoi; Writing – review and editing: Ho Tan Thanh, Dang Dinh Khoi, Nguyen Quang Long; Resources: Ho Tan Thanh, Dang Dinh Khoi; Supervision: Nguyen Quang Long. All authors read and agreed to the final version of this manuscript for publication.

■ REFERENCES

[1] Almaquer, F.E.P., Pacatang, F.J.P., Pagulong, J.E.H., and Catulay, A.J.P., 2020, Decolorization of methylene blue dye in distilled and river water samples using citrate-stabilized silver nanoparticles, *Philipp. Sci. Lett.*, 13 (1), 54–60.

[2] Rafatullah, M., Sulaiman, O., Hashim, R., and Ahmad, A., 2010, Adsorption of methylene blue on low-cost adsorbents: A review, *J. Hazard. Mater.*, 177 (1-3), 70–80.

[3] Li, S., Cui, Y., Wen, M., and Ji, G., 2023, Toxic effects of methylene blue on the growth, reproduction and physiology of *Daphnia magna*, *Toxics*, 11 (7), 594.

[4] Soltanian, S., Gholamhosseini, A., and Banaee, M., 2021, Effects of exposure to a therapeutic level of methylene blue on antioxidant capacity, haemato-immunological responses and resistance of goldfish, *Carassius auratus* to *Aeromonas hydrophila*, *Aquacult. Res.*, 52 (6), 2640–2650.

[5] Perlberg, S.T., Diamant, A., Ofir, R., and Zilberg, D., 2008, Characterization of swim bladder non-inflation (SBN) in angelfish, *Pterophyllum scalare* (Schultz), and the effect of exposure to methylene blue, *J. Fish Dis.*, 31 (3), 215–228.

[6] European Food Safety Authority (EFSA), Penninks, A., Baert, K., Levorato, S., and Binaglia, M., Dyes in aquaculture and reference points for action, *EFSA J.*, 15 (7), e04920.

[7] U.S. Food and Drug Administration, 2022, *Fish and Fishery Products Hazards and Controls Guidance* (June 2022 Ed.), U.S. Food and Drug Administration, Silver Spring, Maryland, US.

[8] Bužga, M., Machytka, E., Dvořáčková, E., Švagera, Z., Stejskal, D., Máca, J., and Král, J., 2022, Methylene blue: A controversial diagnostic acid and medication?, *Toxicol. Res.*, 11 (5), 711–717.

[9] Kathiresan, V., Kansedo, J., and Lau, S.Y., 2018, Efficiency of various recent wastewater dye removal methods: A review, *J. Environ. Chem. Eng.*, 6 (4), 4676–4697.

[10] Pérez-Botella, E., Valencia, S., and Rey, F., 2022, Zeolites in adsorption processes: State of the art and future prospects, *Chem. Rev.*, 122 (24), 17647–17695.

[11] Kordala, S., and Wyszkowski, M., 2024, Zeolite properties, methods of synthesis, and selected applications, *Molecules*, 29 (5), 1069.

[12] Le, V.D., Mai, T.T., Dang, T.D., and Nguyen, X.T., 2024, Evaluate the adsorption ability of crystal violet in water using synthesised zeolite X materials, *Vietnam J. Sci. Technol.*, 66 (10DB-HH), 56–62.

[13] Thuan, N.M., Linh, N.T.M., Phuong, N.T.T., Duong, N.T.H., Hung, N.M., Tuyet, P.T., Van Dung, N., and Long, N.Q., 2024, Ethanolamine-modified zeolite–chitosan beads as new adsorbents for carbon dioxide capture and crystal violet removal, *Case Stud. Chem. Environ. Eng.*, 10, 100917.

[14] Phuong, N.T.T., Thuan, N.M., Linh, N.T.M., Van Dung, N., Duong, N.T.H., and Long, N.Q., 2024, Effects of organic acids on microwave-assisted leaching for mesopore generation in FAU zeolite, *Appl. Phys. A: Mater. Sci. Process.*, 130 (10), 734.

[15] Ramutshatsha-Makhwedzha, D., Mavhungu, M.L., Baloyi, J., and Mbaya, R., 2025, Synthesis and characterization of Fe_3O_4@TiO_2@Zeolite nanocomposite adsorbent for the removal of levofloxacin antibiotic from environmental water matrices, *J. Iran. Chem. Soc.*, 22 (1), 113–128.

[16] Tubon-Usca, G., Centeno, C., Pomasqui, S., Beneduci, A., and Arias, F.A., 2025, Enhanced adsorption of methylene blue in wastewater using natural zeolite impregnated with graphene oxide, *Appl. Sci.*, 15 (5), 2824.

[17] Daoudi, W., el Mahamdi, M., Dagdag, O., Wan Nik, W.B., Oussaid, A., and El Aatiaoui, A., 2024, Carbon dots: Recent developments and future perspectives, *ACS Symp. Ser.*, 1465, 81–101.

[18] Gengan, S., Ananda Murthy, H.C., Sillanpää, M., and Nhat, T., 2022, Carbon dots and their application as photocatalyst in dye degradation studies – Mini review, *Results Chem.*, 4, 100674.

[19] Wang, Z., Jin, X., Yan, L., Yang, Y., and Liu, X., 2022, Recent research progress in CDs@MOFs composites: Fabrication, property modulation, and application, *Microchim. Acta*, 190 (1), 28.

[20] Jlassi, K., Eid, K., Sliem, M.H., Abdullah, A.M., Chehimi, M.M., and Krupa, I., 2020, Rational synthesis, characterization, and application of environmentally friendly (polymer-carbon dot) hybrid composite film for fast and efficient UV-assisted Cd^{2+} removal from water, *Environ. Sci. Eur.*, 32 (1), 12.

[21] Liu, M.L., Chen, B.B., Li, C.M., and Huang, C.Z., 2019, Carbon dots: Synthesis, formation mechanism, fluorescence origin and sensing applications, *Green Chem.*, 21 (3), 449–471.

[22] Xiao, Y., Wang, Z., Fu, J., Zhang, J., He, Q., Lu, H., Zhou, Q., and Wang, H., 2025, Recent advances in the synthesis, characterization, and application of carbon dots in the field of wastewater treatment: A comprehensive review, *Water*, 17 (2), 210.

[23] Shoaib, A.G.M., Yılmaz, M., El Sikaily, A., Hassaan, M.A., El-Nemr, M.A., and El Nemr, A., 2025, Isotherm, kinetics and ANN analysis of methylene blue adsorption onto nitrogen-doped *Ulva lactuca* biochar, *Sci. Rep.*, 15 (1), 10642.

[24] Chen, W., Zhang, Z., Kang, H., Guo, Y., Pak, T., and Li, G., 2022, On the role of surface functional groups in enhancing methylene blue adsorption by low-temperature biochar derived from *Platanus orientalis* bark, *Desalin. Water Treat.*, 254, 302–312.

[25] Cheung, O., Bacsik, Z., Fil, N., Krokidas, P., Wardecki, D., and Hedin, N., 2020, Selective adsorption of CO_2 on zeolites NaK-ZK-4 with Si/Al of 1.8–2.8, *ACS Omega*, 5 (39), 25371–25380.

[26] Arcibar-Orozco, J.A., Flores-Rojas, A.I., Rangel-Mendez, J.R., and Díaz-Flores, P.E., 2020, Synergistic effect of zeolite/chitosan in the removal of fluoride from aqueous solution, *Environ. Technol.*, 41 (12), 1554–1567.

[27] Liu, X., Liu, Y., and Zhang, T.A., 2021, Preparation of magnetic zeolite/chitosan composite using silane as modifier for adsorption of Cr(VI) from aqueous solutions, *J. Vinyl Addit. Technol.*, 27 (3), 640–654.

[28] Nandiyanto, A.B.D., Ragadhita, R., and Fiandini, M., 2023, Interpretation of Fourier transform infrared spectra (FTIR): A practical approach in the polymer/plastic thermal decomposition, *Indones. J. Sci. Technol.*, 8 (1), 113–126.